Inorg. Chem. **2005**, *44*, 9676–9683

Synthesis, Structure, and Magnetic Properties of Sr_2NiOsO_6 and Ca_2NiOsO_6: Two New Osmium-Containing Double Perovskites

René Macquart,[†] Seung-Joo Kim,[†] William R. Gemmill,[†] Judith K. Stalick,[‡] Yongjae Lee,[§] Tom Vogt,[†] and Hans-Conrad zur Loye*,[†]

Department of Chemistry and Biochemistry, University of South Carolina, Columbia, South Carolina 29208, NIST Center for Neutron Research, National Institute of Standards and Technology, Gaithersburg, Maryland 20899, and Department of Earth System Sciences, Yonsei University, Seoul 120749, South Korea

Received June 24, 2005

Two new double perovskite oxides, Ca_2NiOsO_6 and Sr_2NiOsO_6, have been prepared as polycrystalline powders by solid state synthesis. The two oxides were structurally characterized by variable-temperature powder neutron diffraction. Ca_2NiOsO_6 was found to adopt a monoclinic structure ($P2_1/n$), while Sr_2NiOsO_6 was found to be tetragonal ($I4/m$). Magnetic susceptibility measurements indicate that Ca_2NiOsO_6 orders in a canted antiferromagnetic state at about 175 K while Sr_2NiOsO_6 orders antiferromagnetically at about 50 K.

Introduction

Perovskite oxides containing almost every element in the periodic table have been synthesized, most as simple perovskites, ABO_3, but many as double, $A_2BB'O_6$, triple, $A_3BB'_2O_9$, or other related structures. To date, relatively few osmium oxides have been prepared as perovskites and, in fact, oxides of osmium are perhaps the least investigated of the platinum group metals, and only a limited number of compositions and structure types have been reported. Nonetheless, several interesting structures and properties have been found among the osmium oxides, including superconductivity in the recently reported KOs_2O_6 ($T_c = 9.6$ K)[1] and $RbOs_2O_6$ ($T_c = 6.3$ K)[2] and a metal−insulator transition (225 K) in $Cd_2Os_2O_7$.[3,4] In addition, although the number of osmates is quite limited, a reasonable variety of structures and compositions have been prepared, including several pyrochlores, $Cd_2Os_2O_7$,[3,4] $Tl_2Os_2O_7$,[5] $Hg_2Os_2O_7$,[6] $Ca_2Os_2O_7$,[7−9] $Ln_2Os_2O_7$ (Ln = Pr, Nd, Sm, Eu, Tb, Ho, Lu, Y),[10] simple perovskites, $AOsO_3$ (A = Ca, Sr, Ba),[8,11] and a number of other structure types and compositions, such as M_2OsO_3 (M = Li, Na),[12] $La_4Os_6O_{19}$,[13,14] $La_3Os_2O_{10}$,[15] $NdOsO_4$,[16] M_5OsO_6 (M = Li, Na),[17] Ln_3OsO_7 (Ln = La, Pr, Nd, Sm, Eu, Gd),[18−20] $MOsO_4$ (M = Na, K, Rb, Cs),[21] Cd_3OsO_6,[22] $Sr_{11}Os_4O_{24}$,[23] and the previously mentioned MOs_2O_6 (M = K, Rb).[1,2] Quaternary osmium-containing oxides are even less prevalent and include primarily double perovskites, such as Sr_2MOsO_6 (M = Li, Na, Mg, Ca, Sr, Fe, Co, Sc, Cr, In,

* To whom correspondence should be addressed.
[†] University of South Carolina.
[‡] National Institute of Standards and Technology.
[§] Yonsei University.

(1) Yonezawa, S.; Muraoka, Y.; Matsushita, Y.; Hiroi, Z. *J. Phys.: Condens. Matter* **2004**, *16*, L9.
(2) Yonezawa, S.; Muraoka, Y.; Matsushita, Y.; Hiroi, Z. *J. Phys. Soc. Jpn* **2004**, *73*, 819.
(3) Reading, J.; Weller, M. T. *J. Mater. Chem.* **2001**, *11*, 2373.
(4) Sleight, A. W.; Gillson, J. L.; Weiher, J. F.; Bindloss, W. *Solid State Commun.* **1974**, *14*, 357.
(5) Sleight, A. W.; Gillson, J. L. *Mater. Res. Bull.* **1971**, *6*, 781.
(6) Reading, J.; Gordeev, S.; Weller, M. T. *J. Mater. Chem.* **2002**, *12*, 646.
(7) Shaplygin, I. S.; Lazarev, V. B. *Thermochim. Acta* **1977**, *20*, 381.
(8) Chamberland, B. L. *Mater. Res. Bull.* **1978**, *13*, 1273.
(9) Reading, J.; Knee, C. S.; Weller, M. T. *J. Mater. Chem.* **2002**, *12*, 2376.
(10) Shaplygin, I. S.; Lazarev, V. B. *Mater. Res. Bull.* **1973**, *8*, 761.
(11) Shaplygin, I. S.; Lazarev, V. B. *Russ. J. Inorg. Chem.* **1976**, *21*, 1279.
(12) Lazarev, V. B.; Shaplygin, I. S. *Russ. J. Inorg. Chem.* **1978**, *23*, 802.
(13) Shaplygin, I. S.; Lazarev, V. B. *Dokl. Akad. Nauk SSSR* **1978**, *241*, 420.
(14) Abraham, F.; Trehoux, J.; Thomas, D. *Mater. Res. Bull.* **1977**, *12*, 43.
(15) Abraham, F.; Trehoux, J.; Thomas, D. *J. Solid State Chem.* **1979**, *29*, 73.
(16) Abraham, F.; Trehoux, J.; Thomas, D. *J. Inorg. Nucl. Chem.* **1980**, *42*, 1627.
(17) Betz, T.; Hoppe, R. *Z. Anorg. Allg. Chem.* **1985**, *524*, 17.
(18) Lam, R.; Wiss, F.; Greedan, J. E. *J. Solid State Chem.* **2002**, *167*, 182.
(19) Plaisier, J. R.; Drost, R. J.; IJdo, D. J. W. *J. Solid State Chem.* **2002**, *169*, 189.
(20) Gemmill, W. R.; Smith, M. D.; Mozharivskyj, Y. A.; Miller, G. J.; zur Loye, H.-C. *Inorg. Chem.* **2005**, *44*, 7047.
(21) Levason, W.; Tajik, M.; Webster, M. *Dalton Trans.* **1985**, 1735.
(22) Lazarev, V. B.; Shaplygin, I. S. *Russ. J. Inorg. Chem.* **1979**, *24*, 128.
(23) Tomaszewska, A.; Müller-Buschbaum, H. *Z. Anorg. Allg. Chem.* **1993**, *619*, 1738.

10.1021/ic051045+ CCC: $30.25
Published on Web 11/25/2005

Ga),[24] Ba_2MOsO_6 (M = Pr, Nd, Sm−Lu, Y),[25] Ba_2MOsO_6 (M = Co, Ni),[26] Ba_2MOsO_6 (M = Li, Na),[24,27] Ln_2NaOsO_6 (Ln = La, Pr, Nd),[28] and triple perovskites, such as $Ba_3MOs_2O_9$ (M = Li, Na).[29]

Our group has focused on the synthesis of new platinum-group metal oxides in an effort to investigate both the structural chemistry and the magnetic properties of such compounds.[30−35] We have recently reported on the synthesis of several new osmium-containing oxides including Ba_2MOsO_6 (M = Li, Na),[27] Ln_2NaOsO_6 (Ln = La, Pr, Nd),[28] $Ba_3MOs_2O_9$ (M = Li, Na),[29] and Ln_3OsO_7 (Ln = Sm, Eu, Gd).[20] This paper reports the synthesis of two new osmium-containing double perovskites, Ca_2NiOsO_6 and Sr_2NiOsO_6. The structure determination and magnetic properties of these new oxides are discussed.

Experimental Section

Synthesis. Polycrystalline samples of Ca_2NiOsO_6 and Sr_2NiOsO_6 were prepared via solid-state reactions. Stoichiometric amounts of the starting materials (2 mmol of CaO or SrO, 1 mmol of NiO, and 1 mmol of Os) were mixed in a glovebox and placed in an alumina crucible. The CaO and SrO were obtained from thermal decompositions of $SrCO_3$ and $CaCO_3$ at 1050 °C under vacuum. An appropriate amount (3.5 mmol) of Ag_2O was placed into a separate alumina crucible. The two crucibles were placed into a quartz tube and sealed using a H_2/O_2 flame under a dynamic vacuum of 10^{-4} Torr. The tube was heated at 850 °C for 20 h. Ag_2O decomposed to oxygen and silver metal by the time the reaction temperature was reached. The slight oxygen excess assured that osmium reached its intended oxidation state.

The assumed reaction is as follows

$$2CaO\ (\text{or } SrO) + NiO + Os + 3.5\ Ag_2O \rightarrow Ca_2NiOsO_6\ (\text{or } Sr_2NiOsO_6) + 7Ag + 0.25O_2$$

After being allowed to cool to room temperature, the black powder product was removed from the crucible and characterized by powder X-ray diffraction using a Rigaku D/max 2200 instrument. To prepare the quantity of sample needed for neutron diffraction, the above procedures were repeated four times. The products from all the batches were mixed again with a small amount (2 mol%) of Os metal and heated with the appropriate amount of Ag_2O (1 mmol) in a sealed quartz tube at 850 °C for 20 h. (Some osmium volatization is inevitable and can be corrected via the addition of a small amount of additional osmium metal.) Nearly phase pure Sr_2NiOsO_6 was obtained by this route. Ca_2NiOsO_6 was similarly prepared, although its synthesis required three additional heating/grinding steps. Synthesis of Sr_2NiOsO_6 for the synchrotron powder diffraction measurements was completed in a separate single batch using the method described above.

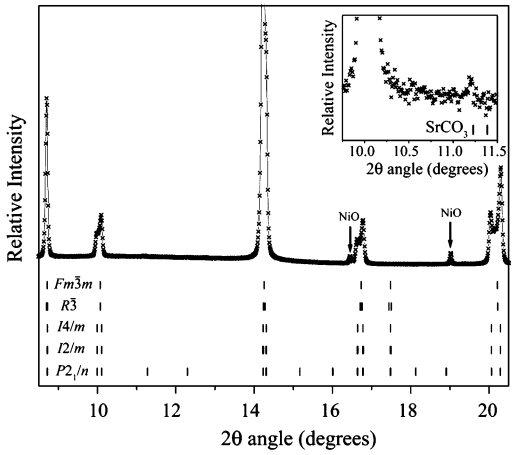

Figure 1. Selected portion of the synchrotron diffraction pattern of Sr_2NiOsO_6 at 300 K showing reflection markers for $Fm\bar{3}m$, $R\bar{3}$, $I4/m$, $I2/m$ and $P2_1/n$ (from top to bottom). NiO ($Fm\bar{3}m$) impurity peaks are indicated. The inset shows reflection markers for $SrCO_3$ (*Pmcn*).

Neutron Powder Diffraction. Neutron diffraction data were collected using 4.0 g samples of Ca_2NiOsO_6 and Sr_2NiOsO_6, contained in 9.5 mm (3/8 in.) diameter vanadium sample cans. A closed cycle He refrigerator was used for temperature control. Patterns were collected using the BT-1 32-detector high-resolution neutron powder diffractometer at the National Institute of Standards and Technology Center for Neutron Research, Gaithersburg, MD. A Cu(311) monochromator with a 90° takeoff angle and 15 min in-pile collimation was used. The neutron wavelength was 1.5402-(1) Å. Data from the 32 detectors were combined to give pseudo-one-detector data over a total scan range of $3° \le 2\theta \le 168°$ with a step size of 0.05° (2θ angle). Structural nuclear and magnetic models were refined using the Rietveld method as implemented in the program GSAS.[36]

X-Ray Powder Diffraction. Both Ca_2NiOsO_6 and Sr_2NiOsO_6 were analyzed for sample purity and cation ordering using a Rigaku D/Max 2200 Cu K_α X-ray powder diffractometer. Additionally, high-resolution X-ray powder diffraction measurements were performed on beamline X7A at the NSLS (National Synchrotron Light Source) at Brookhaven National Laboratories, New York. A dataset was collected at $\lambda = 0.69041(1)$ Å with a step size of 0.01° (2θ angle). A sample of Sr_2NiOsO_6 was housed in a glass capillary of diameter 0.3 mm that was set spinning during data collection in order to minimize the effects of preferred orientation. Structural model refinement was carried out using the same approach as that employed for the neutron data.

Magnetic Susceptibility. Magnetic susceptibility of Ca_2NiOsO_6 and Sr_2NiOsO_6 as a function of temperature was measured using a Quantum Design MPMS XL SQUID magnetometer at applied field strengths of 2 and 1 kG, respectively. Both field-cooled (FC) and zero-field cooled (ZFC) measurements were performed, in the temperature range $2\ K \le T \le 300\ K$ for Ca_2NaOsO_6 and $2\ K \le T \le 350\ K$ for Sr_2NiOsO_6. Magnetization vs field curves were

(24) Sleight, A. W.; Longo, J.; Ward, R. *Inorg. Chem.* **1962**, *1*, 245.
(25) Treiber, V. U.; Kemmler-Sack, S. *Z. Anorg. Allg. Chem.* **1981**, *478*, 223.
(26) Treiber, V. U.; Kemmler-Sack, S. *Z. Anorg. Allg. Chem.* **1980**, *470*, 95.
(27) Stitzer, K. S.; Smith, M. D.; zur Loye, H.-C. *Solid State Sci.* **2002**, *4*, 311.
(28) Gemmill, W. R.; Smith, M. D.; Prozorov, R.; zur Loye, H.-C. *Inorg. Chem.* **2005**, *44*, 2639.
(29) Stitzer, K. E.; El Abed, A.; Smith, M. D.; Davis, M. J.; Kim, S.-J.; Darriet, J.; zur Loye, H.-C. *Inorg. Chem.* **2003**, *42*, 947.
(30) Gemmill, W. R.; Smith, M. D.; zur Loye, H.-C. *J. Solid State Chem.* **2004**, *177*, 3560.
(31) Davis, M. J.; Mugavero, S. J., III; Glab, K. I.; Smith, M. D.; zur Loye, H.-C. *Solid State Sci.* **2004**, *6*, 413.
(32) Stitzer, K. E.; Smith, M. D.; Gemmill, W. R.; zur Loye, H.-C. *J. Am. Chem. Soc.* **2002**, *124*, 13877.
(33) Stitzer, K. E.; El Abed, A.; Darriet, J.; zur Loye, H.-C. *J. Am. Chem. Soc.* **2004**, *126*, 856.
(34) Gemmill, W. R.; Smith, M. D.; zur Loye, H.-C. *Inorg. Chem.* **2004**, *43*, 4254.
(35) Stitzer, K. E.; El Abed, A.; Darriet, J.; zur Loye, H.-C. *J. Solid State Chem.* **2004**, *177*, 1405.
(36) Larson, A. C.; Von Dreele, R. B. *General Structure Analysis System (GSAS)*, Los Alamos National Laboratory Report No. LAUR-86-748, 2004.

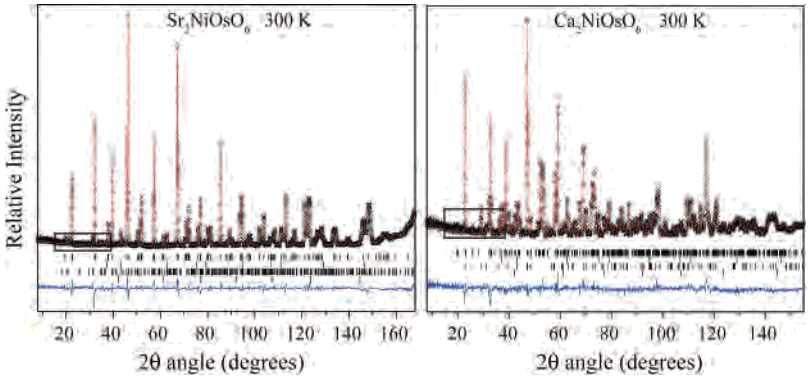

Figure 2. Sample neutron diffraction patterns of Sr_2NiOsO_6 and Ca_2NiOsO_6. The selected area in each case corresponds to the enlarged portions of the diffraction patterns shown in Figure 3. The crosses indicate the data, the red line indicates the calculated model, the blue line at the bottom indicates the difference between the two, and the vertical bars indicate the position of the reflections. In the case of Sr_2NiOsO_6, the upper set of bars correspond to the main phase *I*4/*m* model while the middle sets belong to the NiO and $SrCO_3$ impurity phases. The reflection markers on the right plot correspond to, from top to bottom, Ca_2NiOsO_6 ($P2_1/n$), NiO, and $CaCO_3$. The bottom set of reflection markers in each case correspond to vanadium from the sample canister.

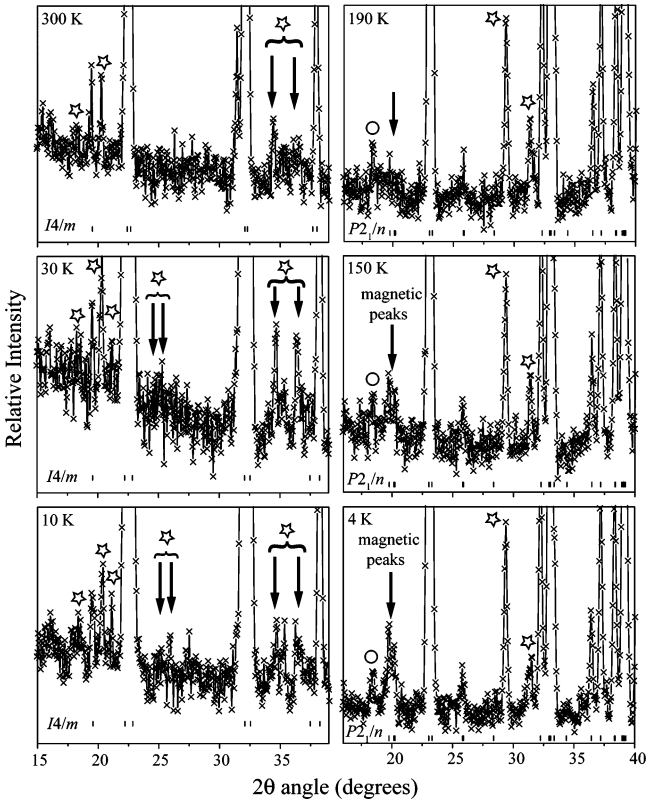

Figure 3. Selected portions of the neutron powder diffraction patterns of Sr_2NiOsO_6 (left) and Ca_2NiOsO_6 (right) showing *I*4/*m* and $P2_1/n$ reflections, respectively. $SrCO_3$ and $CaCO_3$ impurity peaks are marked with a star. Magnetic peak growth is observed at ~20° ($01\bar{1}/011$, $10\bar{1}/101$) for Ca_2NiOsO_6 at 150 and 4 K, while a peak at ~18.3° marked with a circle corresponds to the magnetic 1/2, 1/2, 1/2 reflection of NiO and is observed at all temperatures.

measured between 5 and 200 K in ZFC mode for Ca_2NiOsO_6. The sample was contained in a gelatin capsule fastened in a plastic straw for immersion into the SQUID. No diamagnetic correction was made for the sample container.

Results and Discussion

1. Structure. Neutron powder diffraction was the main tool used in the study of the structure of the A_2NiOsO_6 (A = Ca, Sr) system. In addition to the preliminary laboratory X-ray powder diffraction measurements for both compounds, a single synchrotron X-ray powder diffraction dataset was collected for Sr_2NiOsO_6. Ca_2NiOsO_6 was found to adopt a monoclinic structure in space group $P2_1/n$, which was readily ascertained from the powder neutron diffraction data. The

Table 1. Atomic Coordinates of Sr_2NiOsO_6 as a Function of Temperature Obtained from Synchrotron X-Ray and Neutron Powder Diffraction Data[a]

atom	site	*x*	*y*	*z*	U_{iso} (Å^2)[b]
		Sr_2NiOsO_6 (*I*4/*m*)—synchrotron 300 K			
Sr	4*d*	0	1/2	1/4	0.0097(3)
Ni	2*a*	0	0	0	0.0004(6)
Os	2*b*	0	0	1/2	0.0015(2)
O1	4*e*	0	0	0.2571(13)	0.033(4)
O2	8*h*	0.240(4)	0.273(4)	0	0.049(4)
		Sr_2NiOsO_6 (*I*4/*m*)—neutron 300 K			
Sr	4*d*	0	1/2	1/4	0.0110(3)
Ni	2*a*	0	0	0	0.0050(7)
Os	2*b*	0	0	1/2	0.0049(7)
O1	4*e*	0	0	0.2594(8)	0.0165(6)
O2	8*h*	0.2268(8)	0.2888(7)	0	0.0143(4)
		Sr_2NiOsO_6 (*I*4/*m*)—neutron 30 K			
Sr	4*d*	0	1/2	1/4	0.0050(2)
Ni	2*a*	0	0	0	0.0052(3)
Os	2*b*	0	0	1/2	0.0033(3)
O1	4*e*	0	0	0.2555(8)	0.0088(3)
O2	8*h*	0.2194(3)	0.2968(3)	0	0.0068(2)
		Sr_2NiOsO_6 (*I*4/*m*)—neutron 10 K			
Sr	4*d*	0	1/2	1/4	0.0053(4)
Ni	2*a*	0	0	0	0.007(6)
Os	2*b*	0	0	1/2	0.0015(9)
O1	4*e*	0	0	0.2552(14)	0.0091(5)
O2	8*h*	0.2195(9)	0.2955(9)	0	0.0076(4)

*a*Numbers in parentheses indicate the standard uncertainty in the last digit of the value. Where absent, the value was not refined. [b] Anisotropic thermal parameters calculated for O1 and O2 are shown in Table 2.

Table 2. Refined Anisotropic Thermal Parameters for O1 and O2 of Sr_2NiOsO_6 as a Function of Temperature Obtained from Neutron Powder Diffraction Data[a]

T (K)	atom	U_{11} (Å^2)	U_{22} (Å^2)	U_{33} (Å^2)	U_{12} (Å^2)
300	O1	0.0217(8)	$U_{22} = U_{11}$	0.005(1)	
	O2	0.010(3)	0.008(2)	0.0256(8)	−0.006(1)
30	O1	0.0078(5)	$U_{22} = U_{11}$	0.0118(8)	
	O2	0.0055(6)	0.0050(5)	0.0108(6)	−0.0013(6)
10	O1	0.0078(6)	$U_{22} = U_{11}$	0.013(1)	
	O2	0.015(3)	−0.0018(2)	0.0096(7)	−0.001(1)

[a] Numbers in parentheses indicate the standard uncertainty in the last digit of the value.

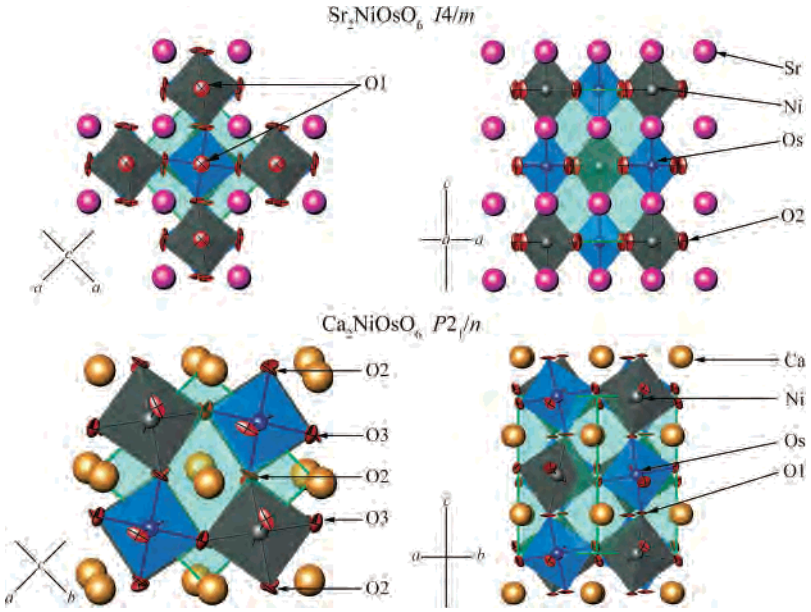

Figure 4. Structural diagrams of Sr_2NiOsO_6 (top) and Ca_2NiOsO_6 (bottom) looking down the [001] axis (left) and [100] axis (top right) of the *I*4/*m* structure and [110] axis (bottom right) of the $P2_1/n$ structure. The gray octahedra represent NiO_6, the blue represent OsO_6, the magenta spheres represent Sr, and the gold spheres represent Ca. Oxygens are shown as red thermal ellipsoids. The green outline indicates the unit cell in each case. Sr_2NiOsO_6 (*I*4/*m*) has the Glazer tilt $a^0a^0c^-$, while Ca_2NiOsO_6 ($P2_1/n$) has the Glazer tilt $a^-a^-c^+$.

Table 3. Lattice Parameters and Refinement Statistics for Sr_2NiOsO_6 (*I*4/*m*) as a Function of Temperature Obtained from Synchrotron X-Ray and Neutron Powder Diffraction Data[a]

sample	*a* (Å)	*c* (Å)	*V* (Å^3)	R_p (%)	R_{wp} (%)	χ^2
300 K synch	5.5377(11)	7.9198(15)	242.87(14)	3.34	5.79	4.87[b]
300 K neutron	5.5326(1)	7.9220(1)	242.49(1)	5.98	7.82	1.76
30 K neutron	5.4947(1)	7.9901(1)	241.24(1)	5.98	8.10	3.47
10 K neutron	5.4947(1)	7.9922(2)	241.30(1)	6.12	8.30	3.58

[a] Numbers in parentheses indicate the standard uncertainty in the last digit of the value. From the 300 K neutron refinement, 0.68(3)% NiO and 1.48(9)% $CaCO_3$ (by weight) were present as impurities in the sample. [b] F^2(%) listed instead of χ^2 which is a large number due, in this case, to an instrumental effect particular to X7A.

structure was refined in space group $P2_1/n$ without difficulty. The structure of Sr_2NiOsO_6, on the other hand, refined well in the tetragonal space group *I*4/*m*. $CaCO_3$ was found to be present in the Ca_2NiOsO_6 sample and $SrCO_3$ in the Sr_2NiOsO_6 sample, while NiO was present in both. Figure 1 shows a portion of the synchrotron diffraction pattern of Sr_2NiOsO_6 obtained at 300 K. Using the methodology outlined in the recent work of Barnes et al.[37] and Lufaso et al.,[38] a model was initially refined in the primitive cubic space group $Pm\bar{3}m$ with the lattice parameter $a \approx 2a_{primitive} = 7.8503$ Å. Cation ordering, indicated by the presence of (odd, odd, odd; $h = k = l$) reflections, suggested that the structure belonged to one of the following space groups: $Fm\bar{3}m$, $R\bar{3}$, *I*4/*m*, *I*2/*m*, *P*4/*mnc*, $P2_1/n$, or $P\bar{1}$. Since Os ($Z = 76$) is a far better scatterer of X-rays than Ni ($Z = 28$) the use of X-ray diffraction and particularly synchrotron X-ray diffraction clearly shows that cation ordering of the Ni^{2+} and Os^{6+} in Sr_2NiOsO_6 does occur, a fact that would not be obvious from the neutron data alone since the neutron scattering lengths are similar for Ni (10.3 fm) and Os (10.7 fm).[39] When the Ni and Os site occupancies were allowed to refine, no signs of cation disorder were found. Similarly, the Ca_2NiOsO_6

Table 4. Atomic Coordinates of Ca_2NiOsO_6 as a Function of Temperature Obtained from Neutron Powder Diffraction Data

atom	site	*x*	*y*	*z*	U_{iso} (Å^2)[b]
		Ca_2NiOsO_6 ($P2_1/n$)—neutron 300 K			
Ca	4*e*	0.9868(9)	0.0536(4)	0.2492(11)	0.0115(6)
Ni	2*d*	1/2	0	0	0.0070(9)
Os	2*c*	1/2	0	1/2	0.0043(7)
O1	4*e*	0.0882(6)	0.4747(6)	0.2434(6)	0.0108(6)
O2	4*e*	0.7106(8)	0.3047(9)	0.0459(6)	0.0084(8)
O3	4*e*	0.1917(8)	0.2141(8)	0.9537(7)	0.0090(9)
		Ca_2NiOsO_6 ($P2_1/n$)—neutron 190 K			
Ca	4*e*	0.9852(9)	0.0545(4)	0.2494(10)	0.0094(7)
Ni	2*d*	1/2	0	0	0.0069(8)
Os	2*c*	1/2	0	1/2	0.0043(7)
O1	4*e*	0.0910(6)	0.4739(6)	0.2430(5)	0.0087(6)
O2	4*e*	0.7097(7)	0.3044(9)	0.0435(6)	0.0063(8)
O3	4*e*	0.1893(8)	0.2145(9)	0.9522(6)	0.0098(9)
		Ca_2NiOsO_6 ($P2_1/n$)—neutron 150 K			
Ca	4*e*	0.9865(9)	0.0555(4)	0.2490(9)	0.0061(6)
Ni	2*d*	1/2	0	0	0.0067(8)
Os	2*c*	1/2	0	1/2	0.0058(8)
O1	4*e*	0.0920(6)	0.4741(6)	0.2424(5)	0.0084(6)
O2	4*e*	0.7103(8)	0.3052(9)	0.0450(6)	0.0071(8)
O3	4*e*	0.1910(8)	0.2137(9)	0.9515(6)	0.0091(9)
		Ca_2NiOsO_6 ($P2_1/n$)—neutron 4 K			
Ca	4*e*	0.9877(8)	0.0567(4)	0.2491(8)	0.0036(5)
Ni	2*d*	1/2	0	0	0.0050(7)
Os	2*c*	1/2	0	1/2	0.0043(6)
O1	4*e*	0.0932(5)	0.4730(6)	0.2416(5)	0.0060(5)
O2	4*e*	0.7105(7)	0.3060(8)	0.0453(5)	0.0058(7)
O3	4*e*	0.1908(7)	0.2145(8)	0.9520(5)	0.0073(7)

[a] Numbers in parentheses indicate the standard uncertainty in the last digit of the value. Where absent, the value was not refined. [b] Anisotropic thermal parameters calculated for O1, O2, and O3 are shown in Table 5.

(37) Barnes, P. W.; Lufaso, M. W.; Woodward, P. M. *Acta Crystallogr.* **2005**, *B* (submitted).
(38) Lufaso, M. W.; Barnes, P. W.; Woodward, P. M. *Acta Crystallogr.* **2005**, *B* (submitted).
(39) *CRC Handbook of Chemistry and Physics*, 85th ed.; CRC Press: Boca Raton, 2004.

Table 5. Refined Anisotropic Thermal Parameters for O1, O2, and O3 of Ca_2NiOsO_6 as a Function of Temperature Obtained from Neutron Powder Diffraction Data[a]

T (K)	atom	U_{11} (Å^2)	U_{22} (Å^2)	U_{33} (Å^2)	U_{12} (Å^2)	U_{13} (Å^2)	U_{23} (Å^2)
300	O1	0.010(1)	0.022(2)	0.003(1)	−0.004(1)	0.003(1)	0.003(2)
	O2	0.006(2)	0.015(3)	0.010(3)	0.000(2)	0.005(1)	0.000(2)
	O3	0.008(2)	0.002(2)	0.016(2)	0.008(2)	0.000(1)	−0.004(2)
190	O1	0.007(1)	0.019(2)	0.001(1)	−0.004(1)	0.000(1)	0.000(2)
	O2	0.002(2)	0.012(3)	0.009(2)	−0.002(2)	0.001(1)	−0.003(2)
	O3	0.012(2)	0.007(3)	0.01(2)	0.003(2)	0.001(1)	−0.003(2)
150	O1	0.004(1)	0.018(2)	0.002(1)	−0.004(1)	−0.001(1)	0.002(2)
	O2	0.003(2)	0.015(3)	0.008(5)	0.000(2)	0.001(1)	−0.002(2)
	O3	0.010(2)	0.010(2)	0.009(2)	0.005(2)	0.001(1)	−0.004(2)
4	O1	0.004(1)	0.015(1)	0.000(1)	−0.001(1)	0.002(1)	−0.004(2)
	O2	0.002(2)	0.015(3)	0.004(2)	0.000(2)	0.002(1)	−0.002(1)
	O3	0.008(2)	0.007(2)	0.007(2)	0.003(2)	0.002(1)	0.001(1)

[a] Numbers in parentheses indicate the standard uncertainty in the last digit of the value.

Table 6. Lattice Parameters and Refinement Statistics for Ca_2NiOsO_6 as a Function of Temperature Obtained from Neutron Powder Diffraction Data

T (K)	a (Å)	b (Å)	c (Å)	β (deg)	V (Å^3)	R_p (%)	R_{wp} (%)	χ^2
300	5.3763(1)	5.5304(1)	7.6448(2)	90.241(2)	227.30(1)	5.51	6.79	1.00
190	5.3699(2)	5.5352(1)	7.6346(2)	90.265(2)	226.93(1)	5.33	6.68	1.24
150	5.3659(2)	5.5388(1)	7.6271(2)	90.275(2)	226.68(1)	5.29	6.63	1.22
4	5.3608(1)	5.5430(2)	7.6176(2)	90.288(2)	226.35(1)	4.80	6.01	1.56

[a] Numbers in parentheses indicate the standard uncertainty in the last digit of the value. From the 300 K refinement, 2.01(8)% NiO and 3.0(2)% $CaCO_3$ (by weight) were present as impurities in the sample.

model refined from laboratory X-ray diffraction data did not show any signs of cation disorder. *I*4/*m* was chosen as the space group most likely to represent the correct structure of Sr_2NiOsO_6 since it represented the highest-symmetry space group that accounted for the observed peak splitting. In Figure 1, this is exemplified by the splitting observed at ∼10° and 16.75°. Closer inspection of the diffraction pattern reveals the presence of small peaks at ∼11.25° that have been attributed to a $SrCO_3$ impurity phase. While $P2_1/n$ also has peaks that nearly coincide with those attributed to $SrCO_3$, the reflections lack the required intensity.

Neutron powder diffraction patterns of Sr_2NiOsO_6 (300 K) and Ca_2NiOsO_6 (300 K) are shown in Figure 2. The boxed areas in Figure 2 correspond to the same regions sampled at 300, 30, and 10 K for Sr_2NiOsO_6 and 190, 150, and 4 K for Ca_2NiOsO_6, Figure 3. The atomic coordinates, lattice parameters, and quality of fit of the refined models for Sr_2NiOsO_6 and Ca_2NiOsO_6 are listed in Tables 1−6. Anisotropic atomic displacement parameters modeled from the neutron diffraction data were refined for the oxygen atoms of both Sr_2NiOsO_6 and Ca_2NiOsO_6, Tables 2 and 5. The structure of Ca_2NiOsO_6 is clearly monoclinic with lattice parameter a less than b and β significantly greater than 90°, Table 6.

Figure 4 shows a comparison of the tetragonal and monoclinic structural models of Sr_2NiOsO_6 and Ca_2NiOsO_6. Red thermal ellipsoids have been used to represent the oxygen atoms and were plotted using the anisotropic atomic displacement parameters given in Tables 2 and 5. The oxygen atoms displace perpendicularly to the direction of the bonding, seen in Figure 4 as an elongation of the position of the atom normal to the line of the bonding and a shortening along the bond length, since the oxygen atoms will have greater freedom to move away from the bond axis. While the particular sensitivity of neutrons to oxygen atoms allowed the refinement of anisotropic displacements, such

Table 7. Selected Bond Distances from the Synchrotron and Neutron Powder Refinements of Sr_2NiOsO_6 and Ca_2NiOsO_6 at Various Temperatures

Sr_2NiOsO_6 tetragonal *I*4/*m* bond distances (Å)				
bonds/ octahedra	300 K synch	300 K neutron	30 K neutron	10 K neutron
Ni−O1 (×2)	2.036(11)	2.055(6)	2.041(7)	2.040(11)
Ni−O2 (×4)	2.014(8)	2.032(6)	2.028(2)	2.023(7)
Os−O1 (×2)	1.923(11)	1.906(6)	1.954(7)	1.957(11)
Os−O2 (×4)	1.911(7)	1.910(6)	1.904(2)	1.907(7)
Ca_2NiOsO_6 monoclinic $P2_1/n$ bond distances (Å)				
bonds/ octahedra	300 K neutron	190 K neutron	150 K neutron	4 K neutron
Ni−O1 (×2)	2.024(4)	2.029(4)	2.033(4)	2.038(4)
Ni−O2 (×2)	2.058(4)	2.053(4)	2.060(5)	2.065(4)
Ni−O3 (×2)	2.066(4)	2.079(4)	2.069(4)	2.071(3)
Os−O1 (×2)	1.924(4)	1.922(4)	1.917(4)	1.911(4)
Os−O2 (×2)	1.928(4)	1.928(4)	1.924(4)	1.921(4)
Os−O3 (×2)	1.922(4)	1.915(4)	1.925(4)	1.920(4)

was not the case for the cations. Attempts to model cation anisotropic displacement parameters led to instability of the refinement and were consequently excluded. Table 7 shows selected bond distances for Sr_2NiOsO_6 and Ca_2NiOsO_6. In the case of Ca_2NiOsO_6, the equatorial M−O2 and M−O3 (M = Ni, Os) bond distances within each octahedra are close to equal length, particularly in the 150 and 4 K cases, presenting almost regular octahedra that adopt an $a^-a^-c^+$ Glazer tilting scheme.[40] The Ni−O bond distances obtained from the neutron data for Sr_2NiOsO_6 and Ca_2NiOsO_6 are close to the literature values of 2.04[41] and 2.06 Å,[42] while the Os−O bond lengths fall within the, admittedly broad, range given for six-coordinate Os environments in the literature (1.895[41]−2.030 Å[42]). The Ni−O bond distances

(40) Glazer, A. M. *Acta Crystallogr.* **1972**, *B28*, 3384.
(41) Shannon, R. D. *Acta Crystallogr.* **1976**, *A32*, 751.
(42) Brown, I. D. http://www.ccp14.ac.uk/ccp/web-mirrors/i_d_brown; April 2005.

Table 8. Octahedral Tilting in Ca_2NiOsO_6 Relative to the Monoclinic [001] and [110] Axes as a Function of Temperature Calculated from Neutron Diffraction Data

T (K)	Ni [001] tilt (deg)	Os [001] tilt (deg)	Ni [110] tilt (deg)	Os [110] tilt (deg)
300	10.28	11.06	14.15	14.88
190	10.40	11.22	14.56	15.36
150	10.37	11.18	14.66	15.54
4	10.35	11.20	14.84	15.82

Table 9. Octahedral Tilting in Sr_2NiOsO_6 (*I*4/*m*) Relative to the Tetragonal [001] Axis as a Function of Temperature Calculated from Neutron Diffraction Data

T (K)	Ni [001] tilt (deg)	Os [001] tilt (deg)
300	6.86	7.29
30	8.53	9.09
10	8.39	8.91

obtained from the synchrotron data deviate from this range, but this is not unexpected given the relative insensitivity of X-rays to oxygen atoms. Bond valence sum (BVS) calculations for the Ni^{2+}-centered octahedra in the monoclinic model vary from 2.06 at 300 K to 2.02 at 4 K (calculated using the SPuDS/TUBERS software package[43]) while in the tetragonal model the values range from 2.12 at 300 K to 2.18 at 10 K. BVS calculations for the Os^{6+}-centered octahedra are not listed due to the unrealistic range of bond valence parameters in the literature for $Os^{6+}-O^{2-}$ systems, as mentioned above. These differences reflect the general lack of $Os^{6+}-O^{2-}$ systems in the literature upon which to base reliable calculations.

Tables 8 and 9 show the tilting in Ca_2NiOsO_6 and Sr_2NiOsO_6, respectively. These were calculated using the corrected equations of Groen et al.[44] and the SPuDS/TUBERS software package.[43] Two tilt systems are described. The first refers to the octahedral tilting about the [001] axis, while the second refers to the tilting about the [110] axis. In the case of Ca_2NiOsO_6, decreasing the temperature tends to increase the monoclinic splitting angle, β, and the system becomes more monoclinic, Table 6. This is observed as an increase in tilting about the [110] axis as the temperature is lowered. The tilting about the [001] axis remains relatively constant with a slight increase from 300 to 190 K. As previously noted by others[45] the smaller octahedron, usually with the smaller cation, has the greater degree of tilt in each case (ionic radius $Ni^{2+} = 0.690$ Å, $Os^{6+} = 0.545$ Å[41]). This same trend is observed for both Ca_2NiOsO_6 and Sr_2NiOsO_6. Calculation of octahedral tilting in the *I*4/*m* model of Sr_2NiOsO_6 (using the O2−Ni−Os and O2−Os−Ni angles in the *ab* plane) shows a noticeable increase in the tilting in both polyhedra from 300 to 30 K then a slight decrease from 30 to 10 K. Once again, the tilting is greater in the smaller Os^{6+}-centered octahedra.

2. Magnetic Properties. 2.1. Sr_2NiOsO_6. The temperature dependence of the magnetic susceptibility for Sr_2NiOsO_6 in an applied field of 1 kG is shown in Figure 5. Fitting the high-temperature susceptibility (150 K ≤ *T* ≤ 350 K) to the Curie−Weiss law results in values of $\mu_{eff} = 3.44\ \mu_B$, $\theta = 27$ K which is lower than the expected value of about 3.99 μ_B (Ni^{2+}: d^8, $S = 1$; Os^{6+}: d^2, $S = 1$) due to spin−orbit coupling, as seen in other osmium double perovskites.[28] The plot exhibits an antiferromagnetic downturn at about 50 K, despite the fact that the positive Weiss constant suggests net ferromagnetic interactions. Sr_2NiOsO_6 exhibits small deviations between ZFC and FC curves below 20 K, which may be attributed to magnetic frustration.

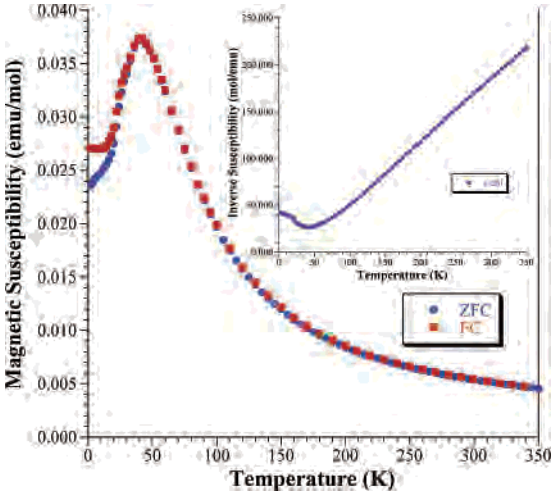

Figure 5. Temperature dependence of the susceptibility of Sr_2NiOsO_6 in an applied field of 1 kG. The inset shows the inverse susceptibility.

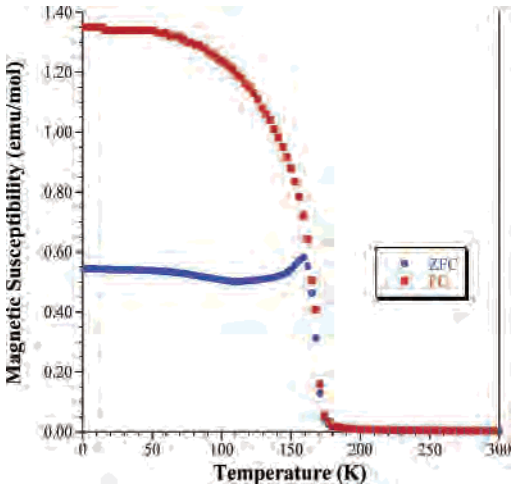

Figure 6. Temperature dependence of the susceptibility of Ca_2NiOsO_6 in an applied field of 2 kG.

2.2. Ca_2NiOsO_6. The temperature dependence of the magnetic susceptibility for Ca_2NiOsO_6 in an applied field of 2 kG is shown in Figure 6. Within the measured temperature range, the high-temperature data could not be fitted satisfactorily to the Curie−Weiss law to calculate the Curie constant or the Weiss constant. At about 175 K, a ferromagnetic-like increase in the susceptibility is observed below which the ZFC and FC data no longer overlay. The field dependencies of the magnetization are shown in Figure 7. Well above the transition temperature (200 K) the plot is linear, indicating paramagnetic-like behavior. However, below 175 K, the field dependencies are no longer linear

(43) Lufaso, M. W.; Woodward, P. M. *Acta Crystallogr.* **2001**, *B57*, 725.
(44) Groen, W. A.; van Berkel, F. P. F.; Ijdo, D. J. W. *Acta Crystallogr.* **1986**, *C42*, 1472.
(45) Mitchell, R. H. *Perovskites: Modern and Ancient*; Almaz Press: Ontario, Canada, 2002; p 318.

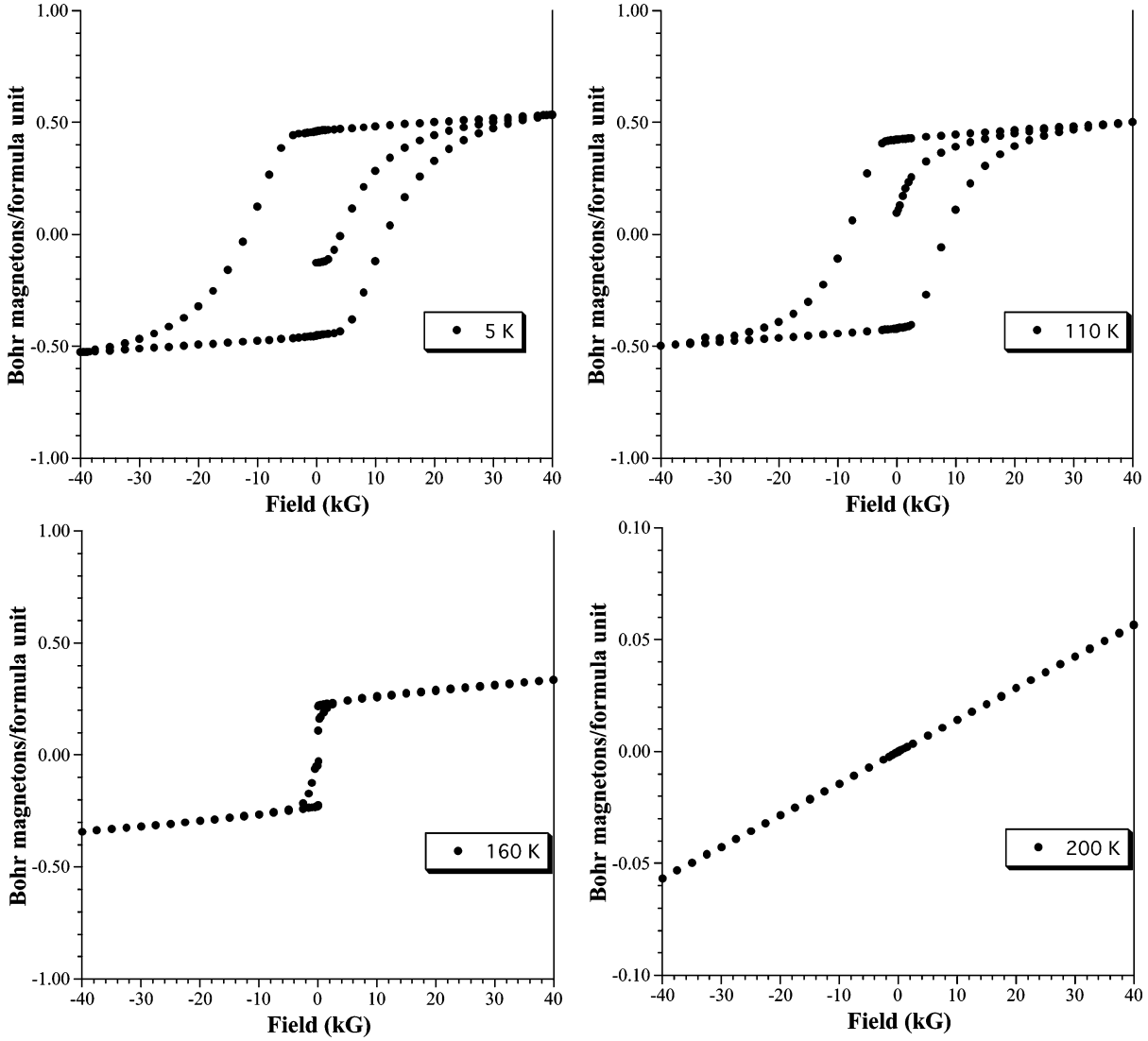

Figure 7. Field dependencies of the magnetization of Ca_2NiOsO_6 measured at 200, 160, 110, and 5 K.

and show ferromagnetic-like behavior down to 2 K. As is readily observed in Figure 7, the remnant magnetization in the field sweep increases with decreasing temperature, as does the coercive field needed to reverse the magnetic moment. The material is not, however, a ferromagnet because the magnitude of the saturation magnetization is too low, measuring only about 0.5 μ_B. For this reason, it is believed that the compound is a canted antiferromagnet with a net moment of $\sim$0.5 μ_B.

It is often possible to determine the magnetic structure using low-temperature powder neutron diffraction data.[46] Intensity due to magnetic neutron scattering is evident in the data collected at 150 and 4 K, predominantly in the weak reflections near 20° 2θ which have little calculated intensity contribution from nuclear scattering, Figure 3. The only marginally observable unique magnetic reflection, at approximately 18.2(2)° 2θ at 4 K, is very small and appears as a shoulder on the magnetic 1/2 1/2 1/2 reflection of the NiO impurity phase. This peak alone is not sufficient to enable the magnetic structure solution but can be indexed by doubling the *b* axis and corresponds to the 110 reflection of the doubled lattice ($2\theta_{calc}$ = 18.4°). If this shoulder is considered to be a real reflection, the magnetic structure can be refined as a canted antiferromagnetic arrangement of spins on the Ni atom positions, with antiferromagnetic ordering along the *c* axis. This model results in a net Ni moment of 2.0(1) μ_B at 4 K and 1.5(2) μ_B at 150 K and calculates intensity for the 110 reflection. However, this model is not proven since a refinement with only ferromagnetic scattering gives identical profile agreement factors with a net Ni moment of 1.7(1) μ_B at 4 K. The canted antiferromagnetic spin model is to be preferred on the basis of the magnetic susceptibility measurements. Note also that no attempt has been made to model the effects of the two Os electrons on the basis of the neutron data due to the dearth of magnetic peaks. Incorporating the moment from these electrons in a canted antiferromagnetic system would likely account for the discrepancy between the Ni-only moment calculated from the neutron data and the net moment resulting from the SQUID measurements.

(46) Martinez-Lope, M. J.; Alonso, J. A.; Casais, M. T. *Eur. J. Inorg. Chem.* **2003**, 2839.

Conclusions

Two new double perovskite osmates, Ca_2NiOsO_6 and Sr_2NiOsO_6, containing Ni^{2+} and Os^{6+} were synthesized as polycrystalline powders, and their structures were determined by neutron and synchrotron powder diffraction. Ca_2NiOsO_6 has monoclinic symmetry ($P2_1/n$) from 300 to 5 K and orders in a canted antiferromagnetic state below about 175 K. Sr_2NiOsO_6 is best refined in space group $I4/m$ from 300 to 10 K. Sr_2NiOsO_6 orders antiferromagnetically below 50 K.

Acknowledgment. Financial support for this research was provided by the National Science Foundation through the Grants DMR: 0134156 and 0450103 and by the Department of Energy through Grant No. DE-FG02-04ER46122. R.M. extends his thanks to M. W. Lufaso for the productive discussions on tilted perovskite systems. Certain trade names and company products are identified in order to specify experimental procedures adequately. In no case does such identification imply recommendation or endorsement by the National Institute of Standards and Technology, nor does it imply that the products are necessarily the best available for the purpose.

Supporting Information Available: Figure of the synchrotron X-ray Rietveld refinement plot of Sr_2NiOsO_6. This material is available free of charge via the Internet at http://pubs.acs.org.

IC051045+